Hybrid multi-walled carbon nanotubes-alginate-polysulfone beads for adsorption of bisphenol-A from aqueous solution

Maria R. Hartono[a,*], Robert S. Marks[a,b,c], Xiaodong Chen[a], Ariel Kushmaro[a,b,c,*]

[a]School of Materials Science & Engineering, Nanyang Technological University, Block N3.1-B3a-02, 50 Nanyang Avenue, Singapore 639798, Singapore, Emails: mrharton1@e.ntu.edu.sg (M.R. Hartono); arielkus@bgu.ac.il (A. Kushmaro)
[b]Avram and Stella Goldstein-Goren, Faculty of Engineering Sciences, The Department of Biotechnology Engineering, Ben-Gurion University of the Negev, P.O. Box 653, Beer-Sheva 84105, Israel
[c]National Institute for Biotechnology Engineering, Ben-Gurion University of the Negev, P.O. Box 653, Beer-Sheva 84105, Israel

ABSTRACT

In recent years, the potential application of carbon nanotubes (CNTs) as sorbent materials in wastewater treatment has garnered tremendous attention. Concerns that CNTs may be toxic to living organism, however, necessitate that the containment of CNTs to prevent their release into the environment in order to realize their practical application in wastewater treatment. In this study, we immobilized multi-walled carbon nanotubes (MWCNTs) within macro-calcium alginate beads. The composite beads were coated with an additional polysulfone (Psf) layer both to provide an external barrier to MWCNTs release into the effluent and also to improve the mechanical integrity of the beads. The hybrid beads were tested for their capacity to remove the bio-refractory endocrine disruptor compound bisphenol-A (BPA) using batch and packed bead column experiments. Maximum BPA removal was achieved at 22% MWCNTs, which was the dispersion limit of MWCNTs in our study. The adsorption of BPA followed Langmuir isotherm model with good correlation. The maximum adsorption capacity of the composite beads of dosage $4\,g\,L^{-1}$ as obtained using the Langmuir model was $24.69\,mg\,g^{-1}$. Addition of the Psf layer, together with MWCNTs, improved the bead compression performance by up to twelvefold at 40% compressive extension. This study showed that the hybrid alginate-Psf bead may serve as compartment for encapsulation of MWCNTs for removal of BPA. Improved compression performance introduced by addition of Psf layer could protect hybrid beads used, for example, in reactors subjected to extreme conditions such as high flow rates.

Keywords: Calcium alginate beads; Adsorption; Bisphenol-A; Multi-walled carbon nanotube; Polysulfone

*Corresponding authors.

1. Introduction

Bisphenol-A (BPA), an endocrine disrupting compound, is a widely used synthesis precursor in the fabrication of polycarbonate and epoxy resins. Owing to its bio-refractory nature, however, its removal from wastewater using conventional treatment processes is difficult. This has led to the common occurrence of BPA in treated effluents of municipal and industrial wastewaters [1,2] which are envisaged as the main sources for the release of BPA into aquatic system [3]. BPA concentrations of up to 17.2 mg/L in waste landfill leachates [4] have been reported. Adsorption is one of the efficient methods for removal of organic pollutants as it is less expensive, simpler, and safer to maintain than membrane filtration and ion-exchange processes [5].

In recent decade, carbon nanomaterials, (CNMs) such as graphene, fullerene, single-walled carbon nanotubes (SWCNTs), and multi-walled carbon nanotubes (MWCNTs), have gained interests in terms of their potential applications as sorbent materials in wastewater treatment due to their high adsorption capacity per unit surface area as well as better adsorption kinetics and re-usability through higher number of cycles in comparison to activated carbon [6]. Myriad of studies have documented the adsorption capacities of these CNMs and its variants towards various organic pollutants [7–10], which in some cases were reported to be higher than activated carbon [9,11] especially for the adsorption of aromatic organic compounds [12]. Their outstanding adsorption properties have been attributed to their hydrophobicity and accessibility of adsorption sites [7]. However, their toxicity effects on human health are still debated [13,14]. Moreover, their lipophilic nature and persistence in the environment may cause them to accumulate along the food chain [9–11]. The application of CNMs as sorbent materials for wastewater treatment, therefore, necessitates the development of suitable compartments to prevent their release into the environment [12].

To date, only few studies addressed the containment of CNMs for their application in water or wastewater treatment to prevent their elution into the effluent [15]. A possible strategy for such containment exploits their entrapment in a hydrophilic alginate matrix. Alginate refers to a family of linear biopolymer arranged of 1,4-linked p-D-mannuronic and a-L-guluronic acid residues [16]. It is able to become cross-linked in the presence of divalent ions such as calcium which results in rapid formation of hydrogels. This property renders them a suitable matrix for immobilization of material by encapsulation [17]. The physical degradation of alginate beads due to abrasion effects, however, has been reported by several authors in different applications [18–21]. This degradation may lead to the eventual release of entrapped materials into the solution. Addition of robust secondary layer onto alginate beads is necessary to provide an additional barrier. Polysulfone (Psf) is a good candidate for secondary layer as it possesses superior mechanical, oxidative, thermal, and hydrolytic stabilities [22]. In addition, several studies have reported the affinity of pollutants with high oil/water partition coefficient towards Psf [23–25].

To the best of our knowledge, the containment of CNMs in double encapsulated beads for removal of pollutant has not been previously explored. In this study, we immobilized MWCNTs, one of CNMs variants, within calcium alginate gel beads which were coated with a Psf layer to provide an additional barrier to MWCNTs release and to improve the bead stability. The simplified illustration of our proposed hybrid Ca-Alg/MWCNTs/Psf bead is shown in Fig. 1.

The hybrid beads were characterized using FTIR, BET surface area analysis, and SEM. The effects of additional Psf layer on the leakage containment of MWCNTs and the stability of the hybrid beads were evaluated by means of bioluminescence toxicity assay and compression test. The batch and column adsorption studies onto the hybrid beads were conducted using synthetic BPA solutions by considering parameters, such as solution pH, adsorbent dosage, initial BPA concentrations, and contact time. The suitability of adsorption models was assessed and maximum adsorption capacity was derived based on Langmuir isotherm model. Adsorption kinetic was studied using pseudo-first- and pseudo-second-order models to determine the rate constants.
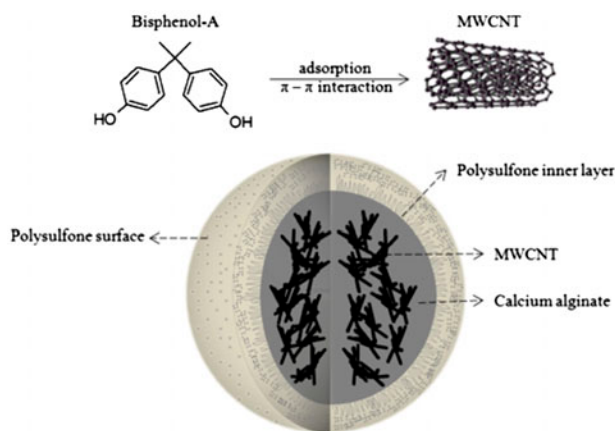
Fig. 1. Simplified illustration of the composite bead with Psf layer (Ca-Alg/MWCNTs/Psf).

2. Experimental materials and methods

2.1. Materials

BPA ((CH$_3$)$_2$C(C$_6$H$_4$OH)$_2$, M_w = 228.3 g mol^{-1}, Sigma, 239658) stock solution of 100 mg L^{-1} was prepared by stirring BPA in distilled water for 2 d. The pH of the stock solutions and all subsequent dilutions were adjusted to 6.0 with 0.1 M sodium hydroxide and 0.1 M hydrochloric acid. The molecular dimension of BPA was estimated using ACD/3D viewer to be 0.4 × 0.4 × 1.0 nm. MWCNTs, Showa Denko VGCF-X, low viscosity alginic acid (Alg, Sigma, A2158), calcium chloride (Sigma, C2661), Psf (Sigma, 428302), N,N-dimethylformamide (N,N-DMF, Sigma, D4551), and Luria Bertani broth (Sigma, L3022) were used in this study. All chemicals were of analytical grade.

2.2. Fabrication of composite beads

Calcium alginate–MWCNTs composite beads (Ca-Alg/MWCNTs) were prepared by adding a known amount of MWCNTs into 2.5-wt.% alginate solution as seen in Table 1. This was followed by sonication (Elmasonic) and overnight stirring. The resulting mixture was dripped into a magnetically stirred 0.5 M calcium chloride solution using a syringe pump (KDS) at 50 mL/h through a polyurethane tube with a 3.5 mm diameter opening. The beads were to age in the calcium solution overnight, washed and stored in distilled water.

The fabrication procedure for Ca-Alg/MWCNTs beads with Psf layer (Ca-Alg/MWCNTs/Psf) was adapted from Ben-Dov et al. [26] which was based on phase-inversion method [27]. Psf at 10-wt.% was prepared by dissolving Psf pellets into N,N-DMF. Each swollen bead was touched to filter paper and dropped into Psf solution for about 20 s before collection and immersion in distilled water to complete the polymerization. The resulting beads were then washed and stored in distilled water at room temperature. For wet weight to dry weight conversion, several batches of swollen beads (wet weight of each 0.5 g) were prepared and heated at 80°C. The dry to wet weight conversion was calculated by measuring the average of the dry weight divided by the initial wet weight prior to drying. All calculations for data analysis were then performed based on the dry weight of the beads.

2.3. Adsorption experiments

Aliquots of swollen beads were added to BPA solutions at concentrations of 20, 40, 60, 80, and 100 mg L^{-1} in glass containers. For kinetic data, each container was placed in shaker set at 120 rpm and aliquots were taken at each specified time during the course of the experiment at room temperature of 22°C. The BPA removal efficiency was calculated as:

$$R_t\ (\%) = (1 - [BPA]_t/[BPA]_0) \times 100\% \qquad (1)$$

where R_t (%) represents the removal ratio of BPA at time t; [BPA]$_0$ (mg L^{-1}) is initial concentration of the BPA solution; and [BPA]$_t$ (mg L^{-1}) is the concentration of BPA at time t. The adsorption capacity was calculated as:

$$q_t = ([BPA]_t - [BPA]_0) \times V/m \qquad (2)$$

where q_t (mg g^{-1}) represents the amount of BPA adsorbed at time t; V (L) is the volume of the BPA solution; and m (g) is the dry weight of the adsorbent added. Batch experiments were done in duplicate with the value reported as mean of the readings.

2.4. Desorption procedure

The desorption experiment was performed using ethanol. Beads with known adsorbed amounts of BPA were placed in ethanol in a glass container for 5 h at room temperature of 22°C. Percentage of desorption was calculated as:

Table 1
Summary of experimental conditions for bead fabrication

Sample	Volume (mL)	Alginic acid (g)	MWCNTs (mg)	Treatments
Ca-Alg	50	1.25	0	Stir overnight
Ca-Alg/ 2%-MWCNTs	50	1.25	25	Sonicate (2 min)—stir 1.5 h—sonicate 20 min—stir
Ca-Alg/ 7%-MWCNTs	50	1.25	100	overnight—sonicate
Ca-Alg/ 14%-MWCNTs	50	1.25	200	
Ca-Alg/ 22%-MWCNTs	50	1.25	350	

$$\text{Desorption (\%)} = ([BPA]_{liq}/([BPA]_{sol} \times 100\% \qquad (3)$$

where $[BPA]_{liq}$ represents the amount of BPA remaining in the solution (mg) and $[BPA]_{sol}$ refers to the amount of BPA in the adsorbent (mg) $\times 100\%$.

2.5. Column adsorption

Column adsorption studies were performed using column made of borosilicate glass of 1.5 cm internal diameter. The column was filled with the hybrid beads by tapping method until the final beads' height was 12.5 cm. BPA solution of 100 mg L^{-1} concentration was injected in an up-flow direction in order to reduce the channeling effect into the column at flow rate of 0.5 mL min^{-1}. Fraction of the effluent was collected as function of time. Breakthrough curves were constructed by plotting the time against removal efficiency of BPA from the influent. Desorption was conducted by injecting ethanol at flow rate of 0.5 mL min^{-1}. Prior to the start of new cycle, the column was flushed with distilled water to remove traces of ethanol and the remaining solution inside the column was drained by pumping air through the column. All experiments were carried out at ambient conditions.

2.6. Characterization

BPA concentrations were determined using a UV–Vis spectrophotometer (Shimadzu UV3600) at a wavelength of 276 nm [23,28] and the concentration was calculated from a calibration curve. Samples of the composite beads for scanning electron microscope (SEM, JEOL 6360) imagery were prepared by drying the beads in an oven at 80°C, mounting them on a support, and coating them with a platinum layer. Fourier transform infrared spectroscopy (FTIR, Perkin-Elmer Spectrum) was used for detection of the functional groups at transmission spectra in the range of 4,000–500 cm^{-1} at resolution of 4 cm^{-1}. Bead mechanical strength was measured on an Instron 5848 microtester connected to an Instron 5800 control unit using a 50-N load cell. A minimum of six beads were analyzed, for each type of composite bead. Anvil height was adjusted to 2.5 mm for all samples followed by 40% compressive extension. Bead diameters were measured using Mitutoyo micrometer 156-101. Zeta potential measurements were made using Malvern Zetasizer Nano ZS. Calcium alginate beads (Ca-Alg) were crushed into small particles using mortar and pestle followed by drying at 70°C. One gram per liter of Ca-Alg particles and 0.05 g/L MWCNTs were added into tubes containing distilled water of different pH values. The pH of the solution was adjusted using 0.1 M hydrochloric acid or sodium hydroxide. Nitrogen adsorption/desorption measurements were conducted using Quantachrome Nova 3200E. The surface area was measured using BET method and the pore size was estimated using BJH method.

2.7. Probing the leakage of MWCNTs using bioluminescence bacteria

Carbon nanotubes (CNTs) have been suspected to induce oxidative stress which eventually contributed to cell death [29]. In this study, an oxidative stress sensitive recombinant bioluminescence bacteria DPD2511 [30] was used to detect the presence of MWCNTs in the solution. In order to study the effect of addition of Psf layer onto Ca-Alg/22%-MWCNTs beads towards containment of MWCNTs, a total of 10 Ca-Alg/22%-MWCNTs beads with and without the addition of Psf layer were immersed in 2 mL of distilled water and subjected to vigorous vortex at high rate for 10 min. The aliquots before and after vortex were then tested using the DPD2511 assay.

As a control, samples of solutions containing MWCNTs of different concentrations were freshly prepared and sonicated for 1 h in ultrasonic bath before use. The detailed description of growth media and assay for DPD2511 had been described elsewhere [31]. In brief, overnight culture of DPD2511 was diluted with fresh Luria Bertani media without antibiotic to obtain ~10^7 cells/mL and incubated without shaking at 37°C for 1.5 h. Ninety micro liters of this suspension was mixed with 10 µL of samples ($n = 3$) in white, opaque 96-wells microtiter plates and followed by bioluminescence measurement (Luminoskan Ascent, Thermofisher Scientific) for 150 min. Bioluminescence signal produced by the bacteria as a response to the different concentrations of MWCNTs was presented in relative light units (RLU). The induction ratio (IR) was calculated as $IR = RLU_{max,sample}/RLU_{max,blank}$ where $RLU_{max,sample}$ corresponds to the maximum RLU produced by the sample and $RLU_{max,blank}$ refers to maximum RLU produced by the negative control (distilled water). The assays were repeated in triplicate with the values reported as mean of the readings.

3. Results and discussion

3.1. Characterization of the hybrid beads

FTIR spectrums of MWCNTs, Ca-Alg, and Ca-Alg/MWCNTs are shown in Fig. 2. As shown in Fig. 2(a), no significant band is observed for MWCNTs. The IR spectra of Ca-Alg at 3,426, 1,637,
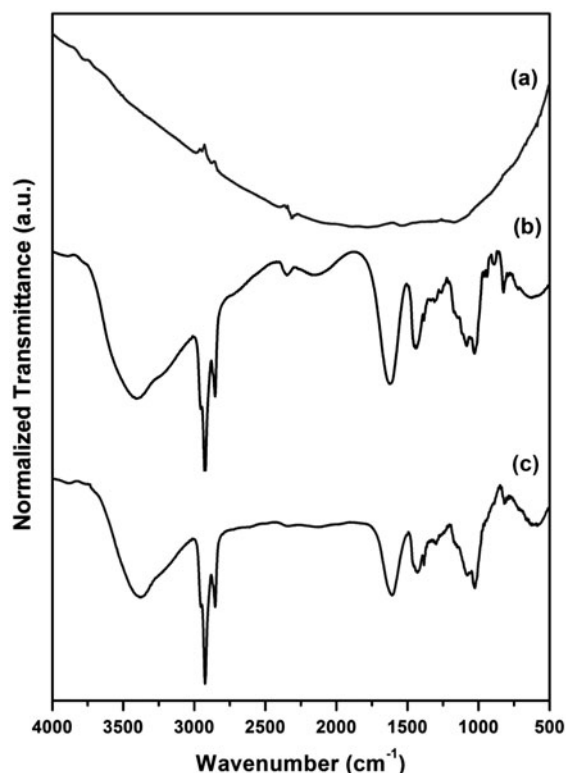
Fig. 2. FTIR spectrum of (a) MWCNTs, (b) Ca-Alg, and (c) Ca-Alg/22%MWCNTs.

1,435, and 1,032 cm^{-1} are contributed by –OH, C=O, C–OH, and OC–OH vibrations. Little discrepancy in the IR spectrum is apparent between Ca-Alg and Ca-Alg/22%-MWCNTs, perhaps due to lower amount of MWCNTs entrapped within the bead.

Fig. 3(a) and (b) shows the SEM images of calcium alginate beads without addition of MWCNTs (Ca-Alg) and calcium alginate beads with addition of MWCNTs (Ca-Alg/MWCNTs). It appears that Ca-Alg/MWCNTs bead has rougher surface in comparison to Ca-Alg. The dimension of MWCNTs used in the study is 10–15 nm in diameter and 3 μm in length. The pore radius of Ca-Alg used in our study was estimated using BJH adsorption method to be 1.67 nm. Hence, it can be assumed that the pore diameter of the Ca-Alg used in our study is less than 10 nm which was sufficient to contain the MWCNTs within the alginate matrix.

It is worth noting that one of the concerns in using solely alginate as entrapment matrix is the possibility of abrasion and the resulted release of the entrapped CNMs. In this study, additional Psf layer is introduced as secondary layer for additional protection and to improve stability. Fig. 3(c) shows the SEM image of the Psf surface on the outer layer of the bead which is covered with polydisperse pores of up to

~10 μm in diameter. To coat the Ca-Alg/MWCNTs bead with Psf, the swollen bead was dropped in Psf solution and then immersed in distilled water which propels the rapid phase separation by means of solvent-outflow and/or non-solvent (water) inflow. Following this rapid exchange, dense skin layers [32] were formed on the outer interface of Psf and another thinner skin layer on the inner interface as Psf solution came into contact with the surface of the swollen alginate surface which was predominantly composed of water with porous structures formed in between these skin layers (Fig. 3(d)). These macrovoid porous structures are covered with pores which resulted from rapid phase separation.

As adsorption occurs mainly in small pores due to their higher surface area and binding affinity for adsorbate, the presence of these pore networks in the Psf layer may improve the adsorption capacity of the bead.

Table 2 shows the comparison of BET surface area values of the beads before and after addition of MWCNTs and Psf layer, respectively. It is shown that addition of MWCNTs and Psf layer increases the surface area of the beads.

3.2. Effect of MWCNTs content

Before addition of Psf layer, batch experiments were performed to select suitable MWCNTs content for Ca-Alg/MWCNTs beads. The MWCNTs at different concentrations were dispersed into 2.5 wt.% alginate solution by varying the total sonication time. Good dispersions were shown up to MWNCTs content of 22% with 40 min of total sonication time. Higher MWCNTs content of 30 and 50% were marked with reduction in the MWCNTs dispersion. This reduction was observed by agglomeration of MWCNTs at the bottom of the vessel which necessitated longer sonication time (Table 3). After 3 h of sonication, the resulted mixture of 30 and 50% MWCNTs became more viscous and difficult to be handled during the injection of the alginate mixture into calcium chloride solution. Due to their viscous nature, the cross-linked composites Ca-Alg/30%-MWCNTs and Ca-Alg/50%-MWCNTs adopted bigger and elongated forms as the contents of MWCNTs increased (Fig. 4).

Since the presence of agglomeration caused frequent inhibition in the syringe's nozzle, in this study the MWCNTs content within Ca-Alg/MWCNTs beads was not increased beyond 22% of MWCNTs. The effects of MWCNTs content immobilized within the alginate beads, without addition of Psf layer, on the removal of BPA are shown in Fig. 5. The BPA
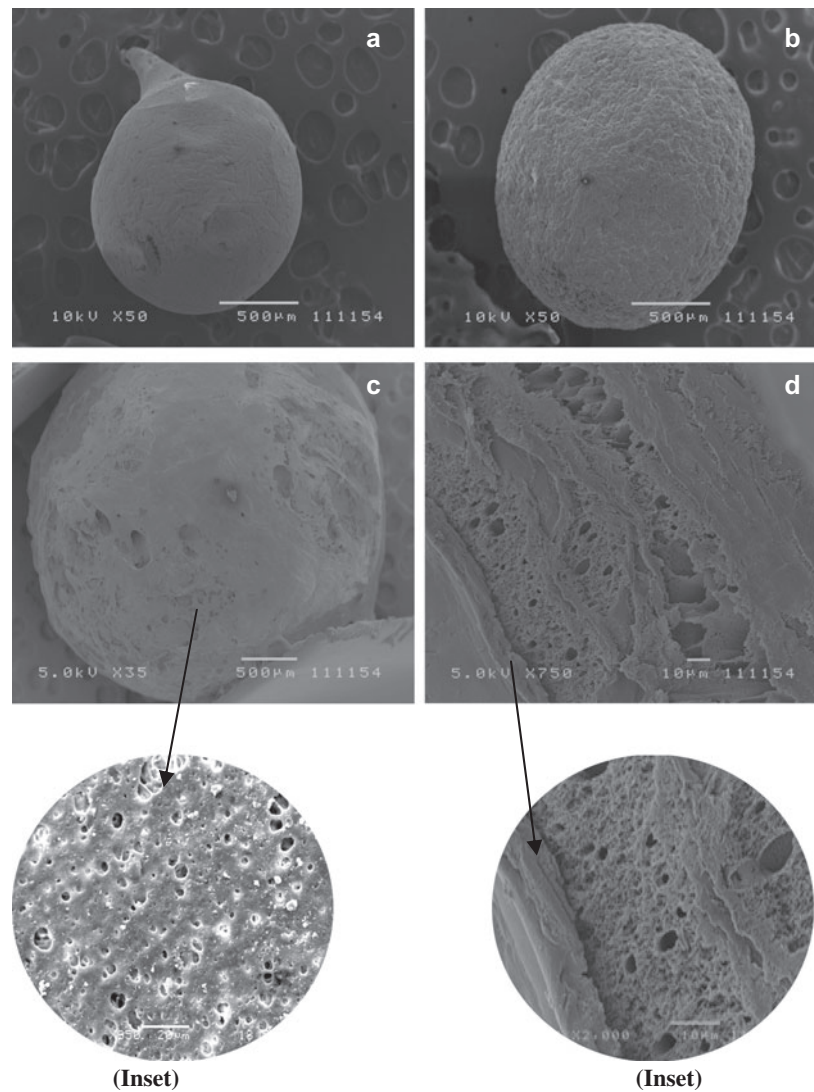
Fig. 3. SEM photographs of (a) surface of Ca-Alg bead, (b) Ca-Alg/ 22%-MWCNTs, (c) Psf surface, and (d) cross-section of Psf layer. Scale bar for (a) and (b) is 500 μm; magnification is 50×; 10 kV. Scale bar for (c) is 35×; 5 kV (inset) is 20 μm; 950×; 10 kV. Scale bar for (d) is 10 μm; 750×; 5 kV (inset) is 10 μm; 2000×; 5 kV.

Table 2
Comparisons of BET surface area values of the hybrid beads

Samples	BET surface area ($m^2 g^{-1}$)
Ca-Alg	2.93
Ca-Alg/ 22%-MWCNTs	18.63
Ca-Alg/ 22%-MWCNTs/Psf	38.71
MWCNTs	325.86

removal efficiency of Ca-Alg/MWCNTs beads is higher than pure Ca-Alg beads but lower than pure MWCNTs. It can be seen that the amount of BPA adsorbed increased with amount of MWCNTs

embedded inside the alginate beads. Hereafter, the Ca-Alg/MWCNTs/Psf beads for subsequent experiment is prepared using Ca-Alg/22%-MWCNTs.

As seen on Fig. 5, the removal rates of Ca-Alg/ MWCNTs beads are inferior in comparison to pure MWCNTs. For pure MWCNTs of the same dry weight dosage, the equilibrium was reached within 1 h of agitation; whereas contact time of more than 4 h was required for equilibrium to be established when MWCNTs were encapsulated within the calcium alginate beads. This result is expected as the porous network of the bead may have limited the diffusion rate of the pollutant [33]. Despite the slower removal associated with the Ca-Alg/MWCNTs beads in

Table 3
Description of MWCNTs dispersion into alginate at different concentration

Content of MWCNTs in alginate	Total sonication time (degree of agglomeration: +, ++, +++)			
	40 min	60 min	2 h	3 h
2%-MWCNTs		← Good dispersion →		
7%- MWCNTs		← Good dispersion →		
14%-MWCNTs		← Good dispersion →		
22%-MWCNTs		← Good dispersion →		
30%-MWCNTs	++	++	+	+
50%-MWCNTs	+++ (thick paste)	+++	+++	+++
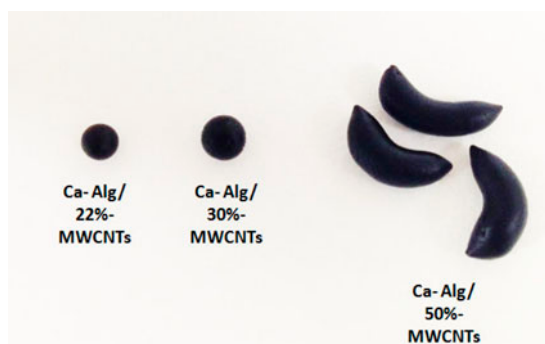
Fig. 4. Structures formed after cross-linking of alginate/ MWCNTs mixture with calcium chloride.
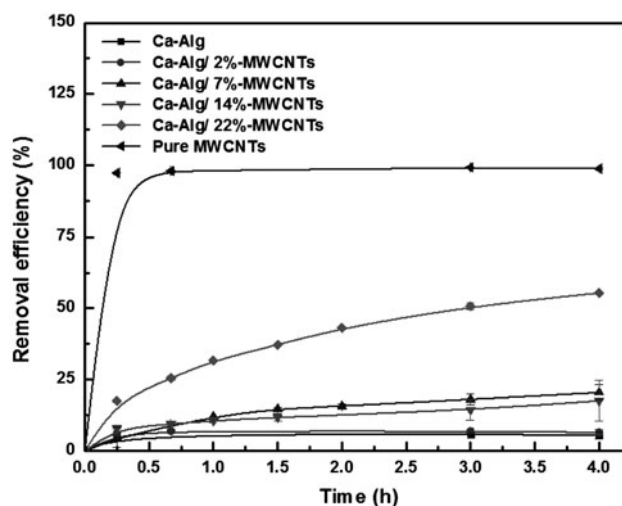
Fig. 5. Effect of amount of MWCNTs immobilized in alginate beads on BPA removal (dosage = 4 g L^{-1} dry weight, pH = 6.0, BPA concentration = 100 mg L^{-1}). Data are expressed as mean ± standard error.

comparison to pure MWCNTs, containment of MWNCTs is still important to prevent its elution into purified effluents.

3.3. Effect of addition of Psf layer

3.3.1. MWCNTs containment

The effect of Psf layer addition on the containment of the MWCNTs was assessed by subjecting Ca-Alg/ 22%-MWCNTs and Ca-Alg/22%-MWCNTs/Psf beads, immersed in distilled water, to high degree of vortex which might have resulted in the abrasion of the beads. The solution was then tested using bioluminescence assay to detect the presence of MWCNTs. The induction factor of bioluminescence released by DPD2511 at different concentrations of MWCNTs is shown in Fig. 6(a). It can be observed that the strain is able to detect the presence of MWCNTs at concentration as low as 10^{-7} µg/mL with maximum induction factor at MWCNTs concentration of 0.005 µg/mL. This finding shows that, indeed, the presence of MWCNTs induces oxidative stress on *Escherichia coli*. The oxidative stress-sensitive DPD2511 strain can therefore be used to imply the presence of MWCNTs in the solution.

Fig. 6(b) shows the induction factor of luminescence released by DPD2511 after its exposure to the aliquots taken before and after vortex. It can be seen that induction factor of the solution immersed with Ca-Alg/22%-MWCNTs beads without addition of Psf layer was higher after vortex, indicating the release of MWCNTs from the bead into the solution; whereas for Ca-Alg/22%-MWCNTs/Psf beads, the induction factor was maintained. Fig. 7(a) and (b) depict the surface of Ca-Alg/22%-MWCNTs beads before and after vortex, it can be seen that several voids were evident on the surface of the beads after vortex due to abrasion.

The results of bioluminescence assay as well as observation of the surface of the beads using SEM indicate that the addition of Psf layer onto Ca-Alg/ MWCNTs beads is beneficial to provide better MWCNTs containment.
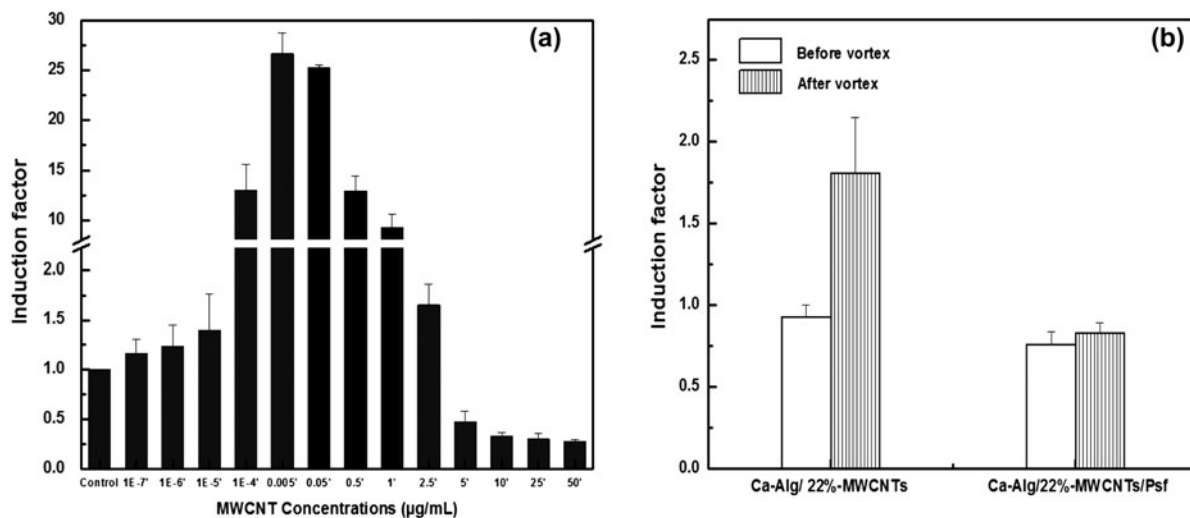
Fig. 6. (a) Induction factor produced by DPD2511 after being subjected to (a) MWCNTs solutions at different concentrations and (b) aliquots taken before and after vortex for Ca-Alg/22%-MWCNTs and Ca-Alg/22%-MWCNTs/Psf beads. Data are expressed as mean ± standard deviation.

3.3.2. BPA adsorption and bead stability

The effect of Psf layer addition on the adsorption of BPA was analyzed by comparing the adsorption capacity of Ca-Alg/MWCNTs and Ca-Alg/MWCNTs/Psf beads with different MWCNTs content at equilibrium (Fig. 8).

It is shown that the addition of the Psf layer to the Ca-Alg/2%-MWCNTs beads resulted in the adsorption of greater amounts of BPA onto Ca-Alg/2%-MWCNTs/Psf beads relative to the Ca-Alg/2%-MWCNTs. In comparison to the more hydrophilic alginate matrix, the hydrophobic property of Psf might

have resulted in higher affinity towards compounds with high K_{ow} and low water solubility, such as BPA which caused the increase in adsorbed BPA amount onto Ca-Alg/2%-MWCNTs/Psf beads. However, the effect of Psf layer addition towards improvement in BPA adsorption is not significant when the MWCNTs content within the beads was increased. As MWCNTs content increased, the effect of MWCNTs as "trap" may have dominated the adsorption process. Therefore, the improvement in BPA adsorption contributed by the addition of hydrophobic Psf layer is less pronounced as the MWCNTs content increased.
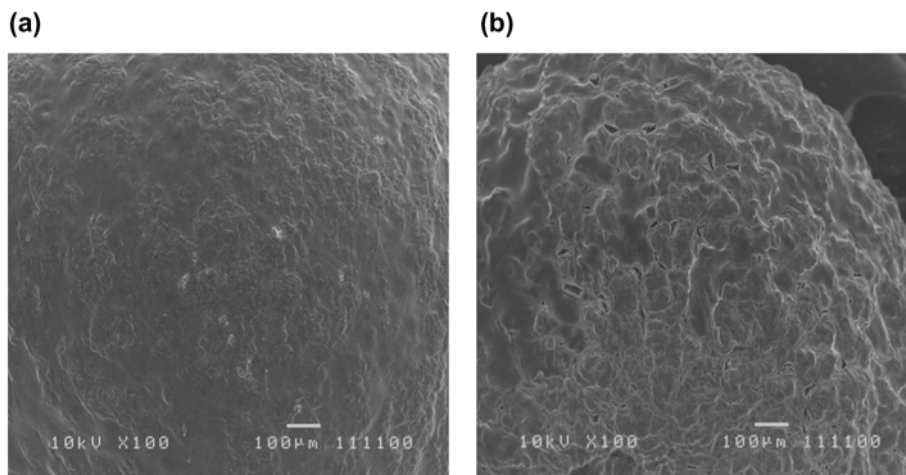
Fig. 7. SEM photographs of (a) surface of Ca-Alg/ 22%-MWCNTs beads (a) before and (b) after vortex. Scale bar for (a) and (b) is 100 μm; magnification is 100×; 10 kV.
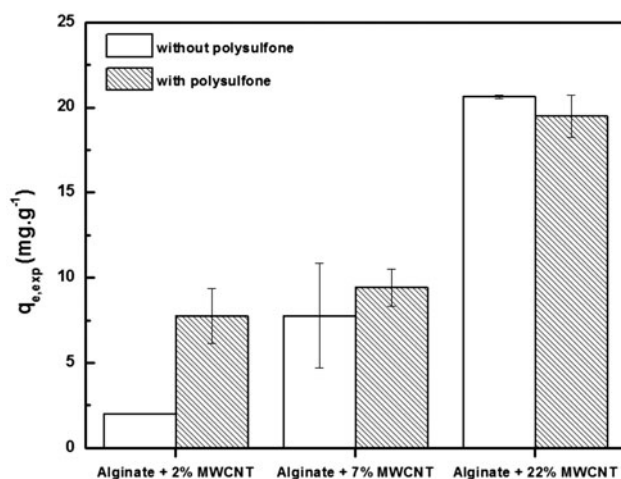
Fig. 8. Equilibrium amounts of BPA adsorbed to Ca-Alg/MWCNTs and Ca-Alg/MWCNTs/Psf. (Dosage = 4 g L^{-1} dry weight, pH = 6.0, BPA concentration = 100 mg. L^{-1}). Data are expressed as mean ± standard error.

Stability of the hybrid beads was examined by means of compression test at 40% compressive extension. Table 4 summarizes the compression property and initial diameter of the hybrid beads before compression.

The results show that compressive load capacity increased with the MWCNTs content added, this observation is in accordance with the previous report which indicated that addition of CNTs as filler improved the mechanical property of hydrogel [34]. The presence of Psf, together with MWCNTs, increases the compressive load capacity at 40% compressive extension up to 12 times in comparison to pure alginate beads.

Although the addition of the Psf layer does not significantly affect the BPA adsorption, especially at higher MWCNTs content, it nevertheless improves the compressive load capacity, and the stability, of the swollen bead.

3.4. Effect of pH on BPA adsorption to Ca-Alg/22%-MWCNT/Psf beads

The pH of the aqueous solution is one of the important parameters affecting the adsorption process because it influences the speciation and the functional groups present in the adsorbate–adsorbent system. The effect of initial solution pH on BPA removal using Ca-Alg/22%-MWCNT/Psf beads) is shown in Fig. 9(a). The pH was ranged from 3 to 11.

The pK$_a$ value for BPA has been reported to be in the range of 9.6–10.2 [35], thus BPA will be negatively charged when pH is higher than pK$_a$ and neutral at pH lower than pK$_a$. From graph 9(a), it can be seen that there is no significant fluctuation of BPA removal observed at pH less than 9, however, the removal efficiency decreased at higher pH.

Zeta-potential measurements of Ca-alginate and MWCNTs particles are shown in Fig. 9(b). The graph shows the trend whereby the surfaces of Ca-alginate and MWCNTs became more negatively charged as the pH increased. Similarly, Psf membrane has also been reported to become more negatively charged with increasing pH [33].

If we consider the behavior of individual components of the bead, namely Ca-alginate, MWCNTs, and Psf which become more negatively charged with increasing pH, then as pH > pKa the electrostatic repulsion effect might have taken place, as the surface of BPA become negatively charged, which resulted in less binding affinity and lower adsorption of BPA onto the hybrid beads.

Based on the experimental results, the solution pH of subsequent experiments in this study was adjusted to 6.0, which is lower than the pKa of BPA. Hence, it can be assumed that there was no net electrical charge in the BPA molecules and that the BPA adsorption onto the hybrid bead occurred mainly via non-electrostatic interaction, namely hydrophobic affinity with Psf and π–π electron coupling between MWCNTs and the π-electrons of the aromatic compounds [7,9].

Table 4
Physical properties of the hybrid beads

Sample	Compressive load at 40% extension (N)	Bead diameter (mm)[a]
Ca-Alg	1.10 ± 0.02	3.37 ± 0.02
Ca-Alg/Psf	6.46 ± 0.39	4.00 ± 0.04
Ca-Alg/ 7%-MWCNTs	1.85 ± 0.07	3.59 ± 0.06
Ca-Alg/ 7%-MWCNTs/Psf	13.48 ± 1.01	3.92 ± 0.06
Ca-Alg/ 22%-MWCNTs	3.38 ± 0.2	3.53 ± 0.03
Ca-Alg/ 22%-MWCNTs/Psf	12.95 ± 0.96	4.04 ± 0.07

[a]Un-contracted beads were used for measurement.
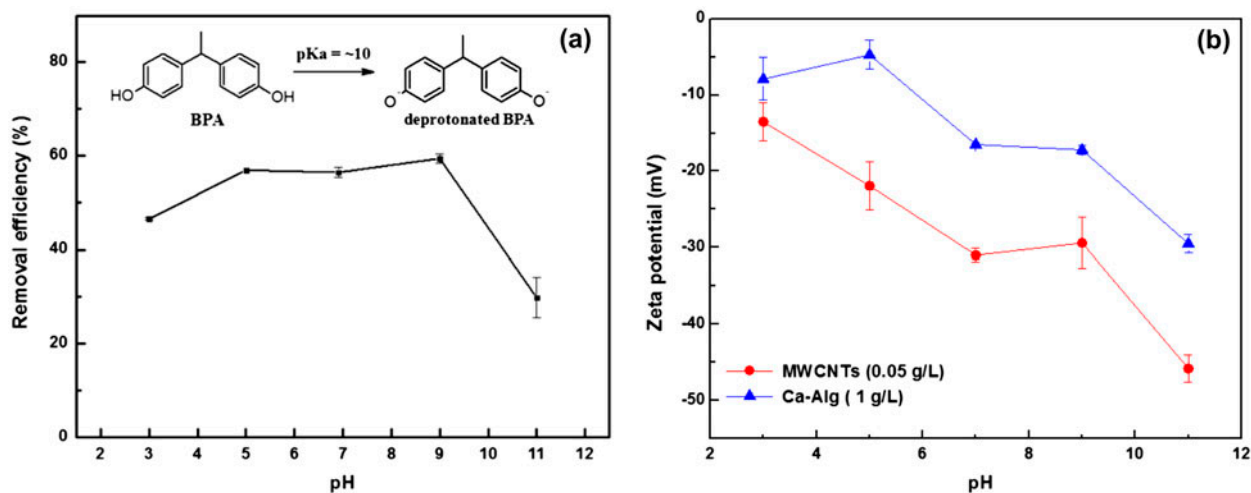
Fig. 9. (a) The effect of pH on BPA removal using Ca-Alg/ 22%-MWCNTs/Psf beads (Dosage = 4 g L^{-1} dry weight, BPA concentration = 100 mg. L^{-1}) (b) Zeta-potential curves vs. pH of Ca-alginate (▲) and MWCNTs (●)Data are expressed as mean ± standard error.

3.5. Effect of Ca-Alg/22%-MWCNT/Psf beads' dosage on BPA adsorption

Effect of hybrid beads' dosage on the removal of BPA is shown in Fig. 10. Experimental studies were conducted at room temperature with 100 mg L^{-1} BPA concentration using contact time of more than 72 h to ensure that equilibrium condition was achieved.

It is evident that removal of BPA increased with increasing dosage from 2 to 10 g L^{-1} dry weight with no significant increase in removal as the dosage was increased further. At the lowest dosage tested (2 g L^{-1}
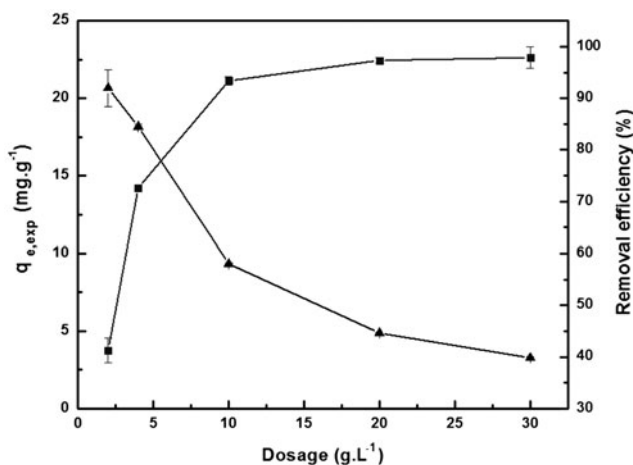
Fig. 10. The effect of adsorbent dosage on the adsorption of BPA onto Ca-Alg/ 22%-MWCNTs/Psf beads at equilibrium (pH = 6.0, BPA concentration = 100 mg L^{-1}, contact time = 141 h), (▲) represents adsorption capacity and (■) denotes %removal. Data are expressed as mean ± standard error.

dry weight), the BPA removal efficiency was 41.3%. Meanwhile at highest dosage (30 g L^{-1} dry weight), the removal efficiency was 97.9%. The higher adsorbent dosage provides more surface active sites available for adsorption. Further increase in adsorption active sites, by increasing the dosage, produces no substantial effect after equilibrium is reached.

3.6. Adsorption kinetic

The adsorption kinetic depicts the rate of BPA adsorption on the hybrid beads which controls the time to reach equilibrium. It is one of the important considerations in designing water treatment process as the kinetic parameters can be used for predicting the adsorption rate and selecting the optimum conditions for the operation of full-scale batch process. The adsorption kinetic could be distinguished into different stages: surface adsorption and rapid external diffusion occurs at the initial stage of adsorption, which is indicated by curved portion in the plot of adsorption capacity against time. The subsequent linear portion in the plot is attributed to steady intraparticle diffusion. The plot reaches plateau when the adsorbate–adsorbent system is in equilibrium as the intraparticle diffusion decreases due to fewer available adsorption sites and low concentration of adsorbate remaining in the solution [36].

The effect of contact time on the adsorption of 100-mg L^{-1} BPA onto Ca-Alg/22%-MWCNT/Psf beads with dosage of 4 g L^{-1} dry weight was analyzed and shown in Fig. 11.
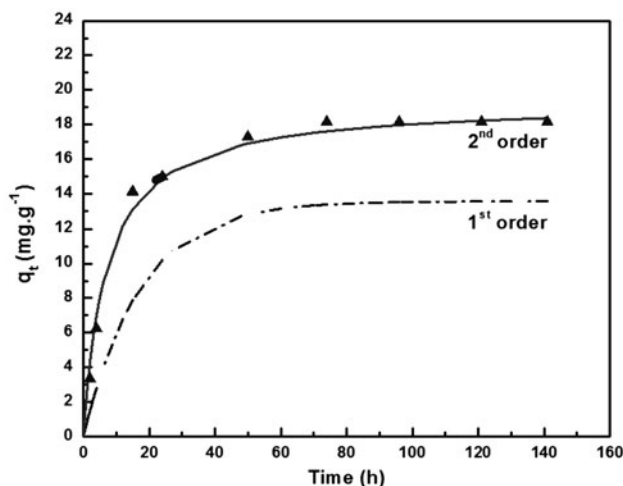
Fig. 11. Effect of contact time on the adsorption of BPA on the Ca-Alg/ 22%-MWCNTs/Psf beads (Dosage = 4 g L^{-1} dry weight, pH = 6.0, BPA concentration = 100 mg L^{-1}), the dotted line and solid lines correspond to simulations based on pseudo-first-order and pseudo-second-order models.

The adsorption capacity of the hybrid beads rose rapidly in the first 40 h and then increased at slower rate until the equilibrium was reached within 72 h. The lengthy contact time required to achieve equilibrium might have been due to the very slow diffusion of the BPA compound from the solution into the porous network of Psf and alginate. Based on the result, a contact time of more than 72 h was chosen in all experiments conducted in this study to ensure that adsorption equilibrium is established.

To understand the mechanism of the adsorption, the data were analyzed by using two widely used kinetic models, namely, pseudo-first-order and pseudo-second- order [37,38].

The pseudo-first-order model is formulated as:

$$\ln(q_{e,\exp} - q_t) = \ln q_{e,\text{cal}} - k_1 t \tag{4}$$

where $q_{e,\exp}$ (mg g^{-1}) is experimental adsorption capacity of the composite bead for BPA at equilibrium; q_t (mg g^{-1}) is the amount of BPA adsorbed at time t (h); $q_{e,\text{cal}}$ (mg g^{-1}) is the adsorption capacity of composite beads calculated using the models; k_1 (h^{-1}) is the rate constant for the pseudo-first-order model. Values of $q_{e,\text{cal}}$ and k_1 for the pseudo-first-order model are obtained from the slope and intercept of the linear plot $\ln(q_{e,\exp} - q_t)$ over time. The pseudo-second-order model is presented as:

$$t/q_t = 1/(k_2 q_{e,\text{cal}}^2) + t/q_{e,\text{cal}} \tag{5}$$

$$h = k_2 q_e^2 \tag{6}$$

where $q_{e,\exp}$ (mg g^{-1}), q_t (mg g^{-1}) and $q_{e,\text{cal}}$ (mg g^{-1}) are the same as described in pseudo-first-order model with h (mg g^{-1} h^{-1}) and k_2 (g mg^{-1} h^{-1}) are the initial sorption rate and the rate constants for pseudo-second-order model. In the pseudo-second-order model, the values for $q_{e,\text{cal}}$ and k_2 are derived from the slope and intercept of plot t/q_t vs. t. Table 5 and Fig. 12 show the calculated kinetic parameters and plots of t/q_t against t for BPA adsorption onto Ca-Alg/ 22%-MWCNT/Psf beads (dosage = 4 g L^{-1} dry weight, pH = 6.0) at different initial BPA concentrations.

High correlations ($R^2 > 0.95$) were obtained for both kinetic models. However, the calculated equilibrium adsorption capacity obtained from the pseudo-second-order model is closer to the experimental adsorption capacity in comparison to the equilibrium adsorption capacity calculated using pseudo-first-order model. The results suggest that the pseudo-second-order model could be employed to represent the adsorption of BPA onto the hybrid beads better than the pseudo-first-order model.

It is observed that when the initial BPA concentration was increased, the pseudo-second-order rate constant (k_2) decreased, while the initial adsorption rate (h) increased, which suggested that concentration of both adsorbate and adsorbent was involved in a rate-determining step.

Weber–Morris kinetic model [39] was utilized to probe further the rate-controlling steps in the adsorption process of BPA onto the hybrid beads. The Weber–Norris kinetic model is described as follows:

$$q_t = K_d t^{0.5} + I \tag{7}$$

where K_d (mg g^{-1} h$^{-0.5}$) represents the rate constant for the intra-particle diffusion and value of I (mg g^{-1}) give insight on the effect of the boundary layer. When a plot of q_t vs. $t^{0.5}$ is linear, it means that intra-particle diffusion was involved in the adsorption process. In addition, if the plot passes through the origin, the intra-particle diffusion can be regarded as a rate-determining step [40].

Fig. 13(a) shows the plot of q_t against $t^{0.5}$ for the Ca-Alg/22%-MWCNT/Psf beads (dosage = 4 g L^{-1} dry weight, pH = 6.0, BPA concentration of 100 mg L^{-1}), it can be observed that the plot could be divided into three linear portion representing different sorption processes, namely: external mass transfer ($K_{d1} = 4.346$ mg g^{-1} h$^{-0.5}$), intra-particle diffusion ($K_{d2} = 0.9987$ mg g^{-1} h$^{-0.5}$), and active sites binding. Since the active

Table 5
Kinetic parameters for BPA adsorption by Ca-Alg/ 22%-MWCNTs/Psf at different initial BPA concentrations (dosage = 4 $g L^{-1}$ dry weight, pH = 6.0)

Concentration of BPA (mg·L^{-1})	$q_{e,exp}$ (mg g^{-1})	Pseudo-first-order				Pseudo-second-order			
		$q_{e,cal}$ (mg g^{-1})	k_1 (h^{-1})	R^2		$q_{e,cal}$ (mg g^{-1})	k_2 (g mg^{-1} h^{-1})	h (mg g^{-1} h^{-1})	R^2
100	18.16	13.6	0.058	0.9626		19.31	0.007	2.734	0.9993
60	12.69	9.11	0.052	0.9847		13.37	0.012	2.125	0.9997
20	4.75	4.11	0.082	0.9972		4.96	0.040	0.990	0.9994
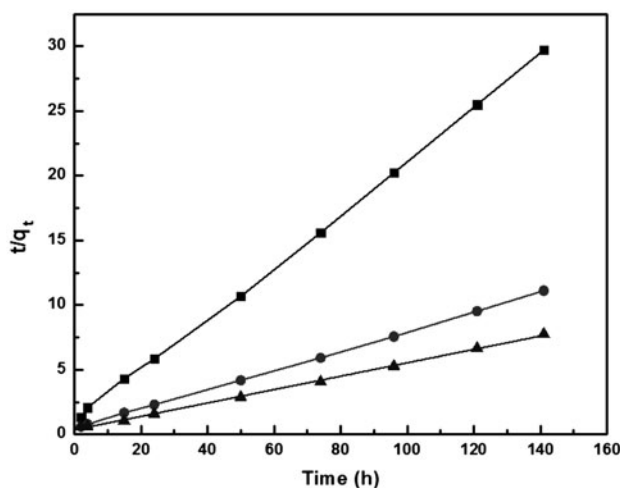
Fig. 12. Pseudo-second-order kinetic plots for the adsorption of BPA on Ca-Alg/ 22%-MWCNTs/Psf beads (dosage = 4 $g L^{-1}$ dry weight, pH = 6.0) at BPA concentrations of (■) 20 mg L^{-1}, (●) 60 mg L^{-1} and (▲) 100 mg L^{-1}. Data are expressed as mean.

sites binding was considered to have occurred rapidly, it could not be a rate-determining step which left intra-particle diffusion and external mass transfer as probable rate-controlling processes involved in the adsorption system.

The plot on Fig. 13(a) does not pass through the origin which suggested that although intra-particle diffusion was involved in the adsorption process, it was not the initial rate-controlling step.

The Boyd plot helps to determine whether the rate-controlling steps are external mass transfer or intra-particle diffusion. The Boyd model [41] is expressed as follows:

$$B_t = -\ln(1 - q_t/q_e) - 0.4977 \quad (8)$$

If the plot of B_t against time passes through the origin, the intra-particle diffusion controls the adsorption otherwise external mass transfer is the rate-controlling

step in the adsorption system. Fig. 13(b) shows the plot of B_t against time for the Ca-Alg/22%-MWCNT/Psf beads (dosage = 4 $g L^{-1}$ dry weight, pH = 6.0, BPA concentration of 100 mg L^{-1}). Similar to Weber–Morris model, the linearized plot did not pass through the origin which implies that external mass transfer was the initial rate-controlling process during the adsorption [42]. Both models infer that the intra-particle diffusion and external mass transfer held important roles in the adsorption of BPA onto the hybrid beads. The desorption of BPA released from the Ca-Alg/22%-MWCNT/Psf beads was estimated by immersing the used hybrid beads with known adsorbed amount of BPA into ethanol. The desorption was estimated to be about 87 ± 4 % (mean ± standard error, $n = 4$), this preliminary result suggested the re-usability potential of the hybrid beads.

3.7. Adsorption isotherm

The adsorption isotherm correlates the concentration of adsorbate in the bulk solution and the amount of solute adsorbed per unit weight of the adsorbent under equilibrium conditions. Correlation between batch equilibrium experimental data and theoretical model is an important consideration as it could be used in the design and analysis of adsorption system. The adsorption isotherm studies were performed at fixed adsorbent dosage of 4 $g L^{-1}$ dry weight by changing the initial BPA concentrations. The equilibrium adsorption of BPA onto Ca-Alg/22%-MWCNT/Psf beads is shown in Fig. 14. It can be observed that the adsorption capacity of the hybrid beads gradually increased with the increasing equilibrium concentration of BPA in the liquid solution as it progressively reached saturation. The equilibrium data were then analyzed using two well-known equilibrium models, Langmuir [43] and Freundlich [44]. The sorption parameters obtained from the models helped to clarify the interaction between the adsorbate and the adsorbent as the system reached equilibrium.
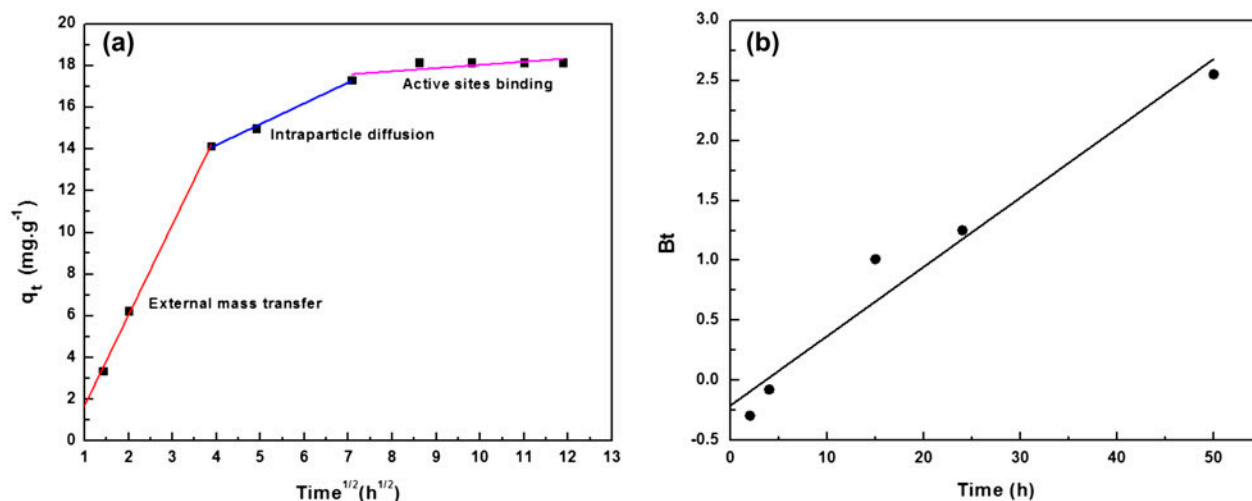
Fig. 13. (a) Weber–Morris graph and (b) Plot of B_t against time for the adsorption of BPA on Ca-Alg/ 22%-MWCNTs/Psf beads (dosage = 4 g L^{-1} dry weight, pH = 6.0 at BPA concentrations of 100 mg L^{-1}). Data are expressed as mean.

Langmuir isotherm is referred as ideal monolayer model as it assumes that the adsorbate molecules formed a monolayer on the energetically identical and structurally homogenous adsorbent sites with the absence of subsequent interactions between adsorbed molecules. The Langmuir model for solid–liquid system is described as:

$$C_{e,exp}/q_{e,exp} = C_{e,exp}/q_m + 1/K_L \qquad (9)$$

$$R_L = 1/(1 + \alpha_L C_o) \qquad (10)$$

where $C_{e,exp}$ (mg L^{-1}) is the equilibrium concentration of BPA in solution; $q_{e,exp}$ (mg g^{-1}) is adsorption of BPA by the composite beads at equilibrium; q_m (mg g^{-1}) is the maximum adsorption capacity of the beads derived from the Langmuir model; R_L is dimensionless equilibrium constant which indicates the shape of the isotherm; K_L (L g^{-1}) and α_L (L mg^{-1}) are the Langmuir coefficients with α_L defined as ratio of K_L over q_m. The Langmuir coefficients, q_m and K_L, are obtained by plotting $C_{e,exp}/q_{e,exp}$ over $C_{e,exp}$.

Freundlich isotherm is based on the assumption that multilayer adsorption on heterogenous surfaces governs the interaction between equilibrium concentration of adsorbate in liquid and solid phase. The Freundlich model is given as:

$$\log q_{e,exp} = (1/n) \times \log C_{e,exp} + \log K_F \qquad (11)$$

where the definition for $C_{e,exp}$ (mg L^{-1}), $q_{e,exp}$ (mg g^{-1}) is the same as described in Langmuir model; K_F (mg$^{1-1/n}$ L$^{1/n}$ g^{-1}) is the Freundlich constant represent-

ing multilayer adsorption capacity and n is a constant representing adsorption strength. The Freundlich coefficients, K_F and n, are obtained by plotting log q_e over log $C_{e,exp}$. For both isotherm models, non-linear method based on trial and error curve-fitting optimization procedure was performed using *solver* add-in with Microsoft's excel to determine the corresponding Langmuir and Freundlich coefficients. The Langmuir and Freundlich parameters for BPA adsorption onto Ca-Alg/ 22%- MWCNTs/Psf beads (dosage = 4 g L^{-1}
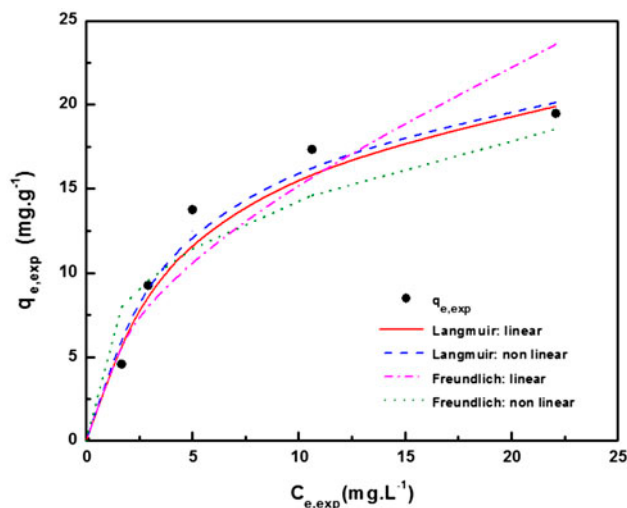
Fig. 14. Isotherm of BPA adsorption onto Ca-Alg/ 22%-MWCNTs/Psf beads (dosage = 4 g L^{-1} dry weight, pH = 6.0, initial BPA concentrations = 20 mg L^{-1}–100 mg L^{-1}). Data are expressed as mean ± standard error.

dry weight, pH = 6.0, BPA concentration = 100 mg L^{-1}) are shown in Table 6.

The calculated n coefficients in both linear and non-linear Freundlich models are between 1 and 10 which inferred favorable adsorption [45]. The results are also supported by the value of the coefficients obtained from Langmuir model. The maximum adsorption capacity q_m of the hybrid beads at adsorbent dosage of 4 g L^{-1} dry weight was predicted using non-linear and linear Langmuir models to be 24.53 mg g^{-1} and 24.69 mg g^{-1}, respectively. R_L value calculated for initial concentration of BPA 100 mg L^{-1} in this study was 0.05, it has been suggested that value of R_L between 0 and 1 indicates favorable adsorption [46].

The adsorption mechanism of BPA on the hybrid beads is complex as the bead is comprised of more than two materials. However, the correlation coefficients attained from both adsorption isotherm models indicated the strong affinity for the BPA adsorption onto the hybrid beads. The correlation coefficients for both linear and non-linear Langmuir model are higher

than the Freundlich model which suggested that Langmuir model fitted the adsorption equilibrium data better and inferred that BPA adsorption by the hybrid beads occurred in a monolayer behavior.

3.8. Column adsorption

The adsorption isotherm data may not be a good representative of scale-up data. To better understand the adsorption behavior of the hybrid beads under continuous flow, a packed bed column was constructed. Continuous flow of 100 mg L^{-1} of BPA was injected to the column for up to 8 h followed by desorption before the subsequent cycle started. The breakthrough curves are shown in Fig. 15.

Since the column study was conducted using high concentration of BPA, it was not possible to remove all of the BPA in the solution initially. Using the current setup (beads height = 12.5 cm and flow rate 0.5 mL min^{-1}, BPA = 100 mg L^{-1}), it appeared that longer contact time was needed for the column to achieve

Table 6
Langmuir and Freundlich parameters for BPA adsorption by Ca-Alg/ 22%- MWCNTs/Psf at equilibrium (dosage = 4 g L^{-1} dry weight, pH = 6.0)

	Langmuir					Freundlich		
	q_m (mg g^{-1})	α_L (L mg^{-1})	K_L (L g^{-1})	R_L	R^2	K_F	n	R^2
Linear	24.69	0.1883	4.650	0.050	0.9808	4.589	1.890	0.9092
Non-linear	24.53	0.2073	5.085	0.050	0.9825	6.745	3.061	0.9297
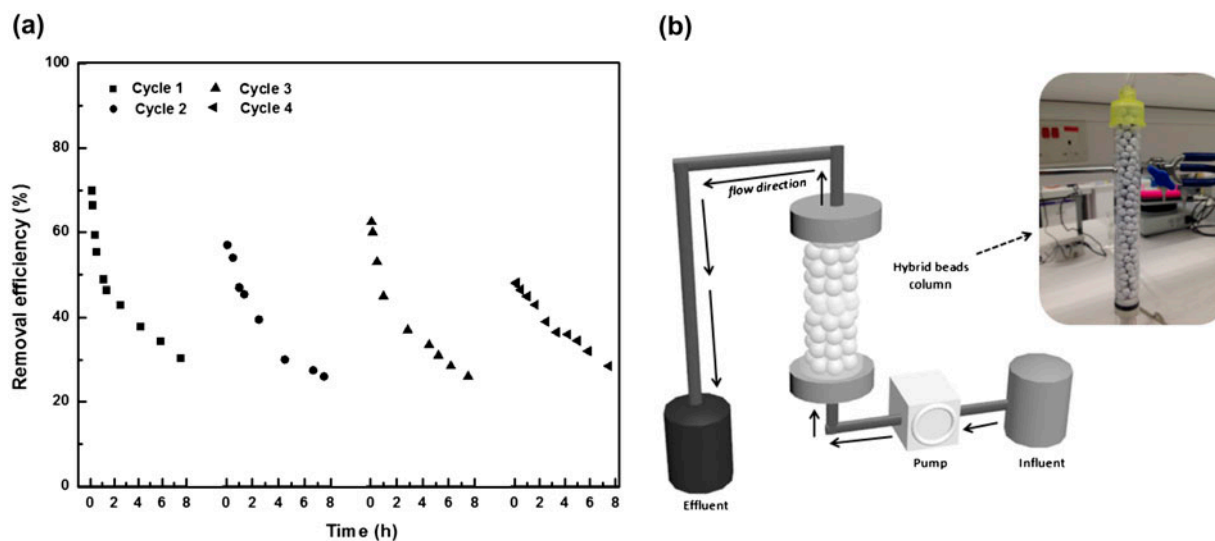
Fig. 15. (a) Breakthrough curve in continuous flow column reactor for adsorption of 100 mg L^{-1} BPA on Ca-Alg/22%-MWCNTs/Psf beads and (b) illustration of up-flow packed bed column setup used in the continuous flow experiment.

complete saturation. Similar removal patterns with slight discrepancies were observed for the first three cycles but at the fourth cycle, the adsorption capacity started to decrease which was indicated by lower removal percentage in the beginning of the cycle. This behavior might be attributed to the decline in desorption efficiency. Nevertheless, the result highlighted the re-usability of the packed hybrid beads column under continuous flow.

4. Summary

A novel hybrid bead comprising of alginate and MWCNTs core, enveloped in a Psf layer was proposed and fabricated in this study. The hybrid beads were investigated for the removal of BPA. The BPA removal increased with the content of MWCNTs. Addition of Psf layer improved the adsorbed BPA amount at lower MWCNTs amount but less significant at higher MWCNTs. The hybrid beads were relatively stable at wide range of pH. The adsorption of BPA by these beads followed pseudo-second-order kinetic and Langmuir isotherm models with high correlation, suggesting monolayer adsorption mechanism. The addition of a Psf layer on composite beads that contained MWCNTs improved the compressive load capacity of the composite beads up to twelvefold at 40% compression. The improved compressive load capacity in beads layered in Psf could be applicable to shield and improve stability of the composite calcium alginate-MWCNTs bead in reactors, whereby the bead sorbents may be subjected to abrasion which could affect the bead integrity.

Acknowledgments

Symbols

R_t	—	removal ratio of BPA at time t, %
$[BPA]_0$	—	initial concentration of the BPA solution, $mg\,L^{-1}$
$[BPA]_t$	—	concentration of BPA at time t, $mg\,L^{-1}$
q_t	—	amount of BPA adsorbed at time t, $mg\,g^{-1}$
V	—	volume of the BPA solution, L
m	—	dry weight of the adsorbent, g
$[BPA]_{liq}$	—	amount of BPA remaining in the solution, mg
$[BPA]_{sol}$	—	amount of BPA in the adsorbent, mg
$q_{e,exp}$	—	experimental adsorption capacity at equilibrium, $mg\,g^{-1}$
$q_{e,cal}$	—	adsorption capacity calculated using the kinetic models, $mg\,g^{-1}$
k_1	—	rate constant for the pseudo-first-order model, h^{-1}
h	—	initial sorption rate for pseudo-second-order model, $mg\,g^{-1}\,h^{-1}$
k_2	—	rate constants for pseudo-second-order model, $g\,mg^{-1}\,h^{-1}$
K_d	—	rate constant for intra-particle diffusion, $mg\,g^{-1}\,h^{-0.5}$
$C_{e,exp}$	—	equilibrium concentration of BPA in solution, $mg\,L^{-1}$
q_m	—	maximum adsorption capacity based on Langmuir model, $mg\,g^{-1}$
R_L	—	Langmuir constant
K_L	—	Langmuir coefficient, $L\,g^{-1}$
α_L	—	Langmuir coefficient, defined as ratio of K_L over q_m, $L\,mg^{-1}$
K_F	—	Freundlich coefficient, $mg^{1-1/n}\,L^{1/n}\,g^{-1}$
n	—	Freundlich constant

References

[1] J. Jackson, R. Sutton, Sources of endocrine-disrupting chemicals in urban wastewater, Oakland, CA, Sci. Total Environ. 405 (2008) 153–160.

[2] A.V. Krishnan, P. Stathis, S.F. Permuth, L. Tokes, D. Feldman, Bisphenol-A: An estrogenic substance is released from polycarbonate flasks during autoclaving, Endocrinology 132 (1993) 2279–2279.

[3] T. Suzuki, Y. Nakagawa, I. Takano, K. Yaguchi, K. Yasuda, Environmental fate of bisphenol A and its biological metabolites in river water and their xeno-estrogenic activity, Environ. Sci. Technol. 38 (2004) 2389–2396.

[4] T. Yamamoto, A. Yasuhara, H. Shiraishi, O. Nakasugi, Bisphenol A in hazardous waste landfill leachates, Chemosphere 42 (2001) 415–418.

[5] M. Grassi, G. Kaykioglu, V. Belgiorno, G. Lofrano, Removal of emerging contaminants from water and wastewater by adsorption process, in: G. Lofrano (Ed.) Emerging Compounds Removal from Wastewater, Springer, The Netherlands, 2012, pp. 15–37.

[6] C. Lu, H. Chiu, H. Bai, Comparisons of adsorbent cost for the removal of zinc (II) from aqueous solution by carbon nanotubes and activated carbon, J. Nanosci. Nanotechnol. 7 (2007) 4–5.

[7] W. Chen, L. Duan, D. Zhu, Adsorption of polar and nonpolar organic chemicals to carbon nanotubes, Environ. Sci. Technol. 41 (2007) 8295–8300.

[8] A.V. Herrera-Herrera, M.Á. González-Curbelo, J. Hernández-Borges, M.Á. Rodríguez-Delgado, Carbon nanotubes applications in separation science: A review, Anal. Chim. Acta 734 (2012) 1–30.

[9] R.Q. Long, R.T. Yang, Carbon nanotubes as superior sorbent for dioxin removal, J. Am. Chem. Soc. 123 (2001) 2058–2059.

[10] C.-Y. Kuo, Comparison with as-grown and microwave modified carbon nanotubes to removal aqueous bisphenol A, Desalination 249 (2009) 976–982.

[11] Y.-H. Li, S. Wang, Z. Luan, J. Ding, C. Xu, D. Wu, Adsorption of cadmium(II) from aqueous solution by surface oxidized carbon nanotubes, Carbon 41 (2003) 1057–1062.

[12] D. Lin, B. Xing, Adsorption of phenolic compounds by carbon nanotubes: Role of aromaticity and substitution of hydroxyl groups, Environ. Sci. Technol. 42 (2008) 7254–7259.

[13] M. Bottini, S. Bruckner, K. Nika, N. Bottini, S. Bellucci, A. Magrini, A. Bergamaschi, T. Mustelin, Multi-walled carbon nanotubes induce T lymphocyte apoptosis, Toxicol. Lett. 160 (2006) 121–126.

[14] J. Muller, F. Huaux, N. Moreau, P. Misson, J.-F. Heilier, M. Delos, M. Arras, A. Fonseca, J.B. Nagy, D. Lison, Respiratory toxicity of multi-wall carbon nanotubes, Toxicol. Appl. Pharmacol. 207 (2005) 221–231.

[15] B. Fugetsu, S. Satoh, A. Iles, K. Tanaka, N. Nishi, F. Watari, Encapsulation of multi-walled carbon nanotubes (MWCNTs) in Ba2+-alginate to form coated micro-beads and their application to the pre-concentration/elimination of dibenzo-p-dioxin, dibenzofuran, and biphenyl from contaminated water, The Analyst 129 (2004) 565–566.

[16] A. Martinsen, G. Skjåk-Bræk, O. Smidsrød, Alginate as immobilization material: I. Correlation between chemical and physical properties of alginate gel beads, Biotechnol. Bioeng. 33 (1989) 79–89.

[17] M. Kierstan, C. Bucke, The immobilization of microbial cells, subcellular organelles, and enzymes in calcium alginate gels, Biotechnol. Bioeng. 19 (1977) 387–397.

[18] J.Q. Albarelli, D.T. Santos, S. Murphy, M. Oelgemöller, Use of Ca–alginate as a novel support for TiO2 immobilization in methylene blue decolorisation, Water Sci. Technol. 60 (2009) 1081–1087.

[19] K.Y. Lee, K.H. Bouhadir, D.J. Mooney, Controlled degradation of hydrogels using multi-functional cross-linking molecules, Biomaterials 25 (2004) 2461–2466.

[20] B. Fouad Sarrouh, D. Tresinari dos Santos, S. Silvério da Silva, Biotechnological production of xylitol in a three-phase fluidized bed bioreactor with immobilized yeast cells in Ca-alginate beads, Biotechnol. J. 2 (2007) 759–763.

[21] C. Vogelsang, R.H. Wijffels, K. Østgaard, Rheological properties and mechanical stability of new gel-entrapment systems applied in bioreactors, Biotechnol. Bioeng. 70 (2000) 247–253.

[22] M.J. El-Hibri, S.A. Weinberg, Polysulfones, in: F.M. Herman (Eds.), Encyclopedia of Polymer Science and Technology, vol. 4, Hoboken, Wiley; 2003, pp. 1–25.

[23] M. Mao, Z. Liu, T. Wang, B. Yu, X. Wen, K. Yang, C. Zhao, Polysulfone-activated carbon hybrid particles for the removal of BPA, Sep. Purif. Technol. 41 (2006) 515–529.

[24] C. Zhao, Q. Wei, K. Yang, X. Liu, M. Nomizu, N. Nishi, Preparation of porous polysulfone beads for selective removal of endocrine disruptors, Sep. Purif. Technol. 40 (2004) 297–302.

[25] W. Su-Hua, D. Bing-zhi, H. Yu, Adsorption of bisphenol A by polysulphone membrane, Desalination 253 (2010) 22–29.

[26] E. Ben-Dov, E. Kramarsky-Winter, A. Kushmaro, An *in situ* method for cultivating microorganisms using a double encapsulation technique, FEMS Microbiol. Ecol. 68 (2009) 363–371.

[27] S. Loeb, S. Sourirajan, Sea Water Demineralization by Means of an Osmotic Membrane, ACS Publications, Washington, DC, 1962.

[28] W.-T. Tsai, C.-W. Lai, T.-Y. Su, Adsorption of bisphenol-A from aqueous solution onto minerals and carbon adsorbents, J. Hazard. Mater. 134 (2006) 169–175.

[29] C.D. Vecitis, K.R. Zodrow, S. Kang, M. Elimelech, Electronic-structure-dependent bacterial cytotoxicity of single-walled carbon nanotubes, ACS Nano 4 (2010) 5471–5479.

[30] T.K. Van Dyk, W.R. Majarian, K.B. Konstantinov, R.M. Young, P.S. Dhurjati, R.A. LaRossa, Rapid and sensitive pollutant detection by induction of heat shock gene-bioluminescence gene fusions, Appl. Environ. Microbiol. 60 (1994) 1414–1420.

[31] F. Li, C. Lei, Q. Shen, L. Li, M. Wang, M. Guo, Y. Huang, Z. Nie, S. Yao, Analysis of copper nanoparticles toxicity based on a stress-responsive bacterial biosensor array, Nanoscale 5 (2012) 653–662.

[32] T. Matsuura, Progress in membrane science and technology for seawater desalination—A review, Desalination 134 (2001) 47–54.

[33] Y. Jodra, F. Mijangos, Phenol adsorption in immobilized activated carbon with alginate gels, Sep. Purif. Technol. 38 (2003) 1851–1867.

[34] X. Tong, J. Zheng, Y. Lu, Z. Zhang, H. Cheng, Swelling and mechanical behaviors of carbon nanotube/poly(vinyl alcohol) hybrid hydrogels, Mater. Lett. 61 (2007) 1704–1706.

[35] C.A. Staples, P.B. Dome, G.M. Klecka, S.T. Oblock, L.R. Harris, A review of the environmental fate, effects, and exposures of bisphenol A, Chemosphere 36 (1998) 2149–2173.

[36] E. Guibal, P. McCarrick, J.M. Tobin, Comparison of the sorption of anionic dyes on activated carbon and chitosan derivatives from dilute solutions, Sep. Purif. Technol. 38 (2003) 3049–3073.

[37] Y.-S. Ho, G. McKay, The kinetics of sorption of divalent metal ions onto sphagnum moss peat, Water Res. 34 (2000) 735–742.

[38] G. Blanchard, M. Maunaye, G. Martin, Removal of heavy metals from waters by means of natural zeolites, Water Res. 18 (1984) 1501–1507.

[39] W.J. Weber, J.C. Morris, Kinetics of adsorption on carbon solution, J. Sanitary Eng. Div. 1 (1963) 1–2.

[40] M. Özacar, I.A. Şengil, Application of kinetic models to the sorption of disperse dyes onto alunite, Colloids Surf. A 242 (2004) 105–113.

[41] G.E. Boyd, A.W. Adamson, L.S. Myers, The exchange adsorption of ions from aqueous solution by organic zeolites II: Kinetics, J. Am. Chem. Soc. 302 (2006) 2836–2848.

[42] V.K. Gupta, A. Mittal, V. Gajbe, J. Mittal, Adsorption of basic fuchsin using waste materials—Bottom ash and deoiled soya—As adsorbents, J. Colloid Interface Sci. 319 (2008) 30–39.

[43] I. Langmuir, The adsorption of gases on plane sur-faces of glass, mica and platinum, J. Am. Chem. Soc. 40 (1918) 1361–1403.

[44] H. Freundlich, Über die adsorption in lösungen [Over the adsorption in solution], J. Phys. Chem. 57(38547) (1906) 1100–1107.

[45] Z. Aksu, Determination of the equilibrium, kinetic and thermodynamic parameters of the batch biosorp-tion of nickel(II) ions onto *Chlorella vulgaris*, Process Biochem. 38 (2002) 89–99.

[46] G. McKay, H. Blair, J. Gardner, Adsorption of dyes on chitin. I. Equilibrium studies, J. Appl. Polym. Sci. 27 (1982) 3043–3057.